IEEE Access
Multidisciplinary | Rapid Review | Open Access Journal

Received April 14, 2020, accepted April 26, 2020, date of publication April 29, 2020, date of current version May 15, 2020.

Digital Object Identifier 10.1109/ACCESS.2020.2991180

45° Linearly Polarized and Circularly Polarized High-Scanning-Rate Leaky-Wave Antennas Based on Slotted Substrate Integrated Waveguide

JIANWEN ZHONG, AMIR KHURRUM RASHID, AND QINGFENG ZHANG, (Senior Member, IEEE)
Department of Electronics and Electrical Engineering, Southern University of Science and Technology, Shenzhen 518055, China

Corresponding author: Qingfeng Zhang (zhang.qf@sustech.edu.cn)

This work was supported in part by the National Natural Science Foundation of China under Grant 61871207, and in part by the Shenzhen Science and Technology Innovation Committee Funds under Grant JCYJ20190809115419425.

ABSTRACT A class of 45° linearly polarized and circular polarized high scanning rate leaky wave antennas are proposed in this paper, which is based on slow-wave substrate integrated waveguide structure. High scanning rate leaky wave antennas have recently become attractive for imaging applications and automotive radar. These applications also require a continuous scanning range without an open stopband, as seen at broadside for ordinary leaky wave antennas. Furthermore, both 45° linearly polarization and circularly polarization are required in practical applications. In this paper, we propose an all-in-one leaky wave antenna design, which features high scanning rate, continuous scanning capability across the broadside, 45° linear polarization or circularly polarization, single-layer configuration, and single-side radiation. Two design examples are provided to illustrate the proposed principle. Both simulation and experimental validation are given.

INDEX TERMS Leaky wave antenna, substrate integrated waveguide, scanning rate, open stopband, linear polarization, circular polarization.

I. INTRODUCTION

Leaky wave antennas (LWAs) belong to a class of travelling wave antennas, which exhibit continuous leakage along their structures. Their attractive features include, frequency dependent beam steering, simple feeding arrangement, broad bandwidth, and an overall low profile structure [1]–[3]. They have been applied in diverse frequency radars [4], spectrogram analysis [5], and mobile communication [6]–[8], etc. They appear applicable to computational imaging, which involves frequency diversity of radiating structures [9]–[12]. In this context, LWAs can be seen as a dispersive metamaterials, whose response changes rapidly with frequency. With a change of frequency, its radiation pattern changes, such that more independent information of the scene can be gathered through a set of finite measurements. In addition to a very high scanning rate, it is also desired that an imaging LWA should be free from the well-known *open stopband* problem. It refers to the very low gain at broadside, when an ordinary LWA scans from backward to forward directions. At that point, most of the supplied energy is actually reflected back to the input port. It may also have a low profile structure, and may use a low-cost technology to realize an economical two-dimensional (2-D) or three-dimensional (3-D) imaging system. Finding the best LWA candidate for imaging applications is an important problem, which invites a new look on LWAs, under a different set of requirements as stated above.

Classical LWAs can be categorized into two major types, having uniform (or quasi-uniform) and periodic structures. For uniform structures, an antenna operates in a fast wave mode, and its main beam scans the forward quadrant only [13]–[15]. On the other hand, periodic LWAs are able to support a scanning both in backward and forward directions. This leads to an increased scanning range of such antennas, making them attractive for imaging applications. However, for periodic LWAs, there exists a well-known common problem of discontinuous scanning, and an *open stopband* around the broadside region is observed.

The associate editor coordinating the review of this manuscript and approving it for publication was Giorgio Montisci.

To close this bandgap for a smooth scanning, different methods have been proposed. These include composite right/left handed (CRLH) transmission line [16]–[19], impedance matching [20], [21], linear curve of phase constant [22]–[24], and asymmetric structures [25]–[27]. In [23], a novel SIW based LWA was proposed, which exhibited a linear curve of phase constant in scanning from backward to forward directions. This was achieved by optimizing the distance between two vias at one lateral wall of a periodically slotted SIW. Ref. [25] has presented an asymmetric structure to overcome the open stopband of a Goubau line based LWA. With transverse and longitudinal asymmetric modulations, the radiation efficiency of this LWA is significantly improved, especially at broadside. However, it scans in an angular span of 40° only, under even a large frequency variation of 4 GHz (from 9 - 13 GHz). Ref. [24] proposes a novel antenna where a single structure is able to generate linear or circular polarization. However, its linear polarization does not offer much control, and instead it is restricted to longitudinal direction only. The structure includes diodes, stubs, and slots to achieve the reported performance. Overall, it is a complicated design, which may be difficult to scale to a different frequency band.

Most of previously reported LWAs use a large frequency variation to achieve a small range of angles. Thus, they are not useful for an imaging application, where scanning rate (defined as the rate of change of main beam direction θ with respect to frequency) is preferred as high as possible [28]. In order to achieve a high scanning rate, a slow wave structure appears an effective way, and some designs have been proposed in [28]–[31]. Ref. [29] uses arrays of transverse metallic blind holes to realize a slow wave effect. However, it requires a complicated fabrication procedure. In [30], slow wave effect has been produced by making closely spaced periodic slots on the top wall of an SIW. Further, a periodic modulation of these slots was also introduced, which led to a higher scanning rate in a narrow bandwidth. Ref. [28] uses a complementary microstrip-slot stubs based structure to realize a high scanning rate LWA. However, the LWAs in [28] and [30] radiate in forward direction only, and there still exists an open stopband around the broadside. The open stopband problem and low scanning rate were both overcome in [31], where high density slots were employed on both faces of SIW.

The frequency scanning feature of LWAs is potentially useful for high-speed microwave imaging and automotive radar. High scanning rate allows the antenna to capture the spatial information using a narrow-band signal only, which greatly eases the A/D converter in baseband system [28]. The suppression of open stopband at the broadside radiation further extends the beam scanning range. In addition to above mentioned features, polarization is also a key parameter that needs to be concerned in microwave imaging and automotive radar. So far, most high scanning rate LWAs dealt with linear polarizations in the horizontal direction only, whereas little works were explored for 45° linearly polarized or circularly polarized high scanning rate LWAs. Vertically placing two identical 45° linearly polarized LWAs, and assigning one for transmitting and the other for receiving, easily forms a two-dimensional microwave imaging aperture [11], which cannot be realized by two horizontally polarized LWAs. Circularly polarized LWAs are also particularly useful for imaging polarization sensitive objects [32], [33].

In this paper, we propose an all-in-one LWA design, which features high scanning rate, continuous scanning capability across the broadside, 45° linear polarization, single-layer configuration, and single-side radiation. Combining two 45° linearly polarized high scanning-rate LWAs with 90° phase difference further forms a circularly polarized high scanning-rate LWA. To the authors' best knowledge, 45° linear polarization and circular polarization are explored for the first time in high scanning-rate LWAs, which will find wide applications in high-speed microwave imaging and automotive radar.

II. PRINCIPLE

A. SCANNING RATE ENHANCEMENT

It is known that frequency dependent beam steering performance of an LWA is caused by the dispersive nature of its propagation constant [1]. $\beta(f)$ is a key parameter for engineering its scanning rate. The angle of main beam from the broadside direction can be estimated as

$$\sin[\theta(f)] = \frac{\beta(f)}{k_0} = \frac{c\beta(f)}{2\pi f}. \tag{1}$$

where $\theta(f)$ is the angle of main beam, and c is the velocity of light in air. For a specific frequency f_0, the main beam scanning rate can be defined as:

$$\nu(f_0) = \frac{d\theta(f)}{df}|_{f=f_0}. \tag{2}$$

where $\nu(f)$ is the scanning rate. Relationship between scanning rate and group velocity can be obtained by substituting (1) in (2), leading to

$$\begin{aligned}\nu(f_0) &= \frac{1}{f\cdot\cos(\theta(f))}\cdot\left[\frac{c}{2\pi}\cdot\frac{d\beta(f)}{df} - \sin(\theta(f))\right] \\ &= \frac{1}{f\cdot\cos(\theta(f))}\cdot\left[\frac{c}{V_g(f)} - \sin(\theta(f))\right]|_{f=f_0}.\end{aligned} \tag{3}$$

where

$$V_g(f) = \frac{d\omega(f)}{d\beta(f)} = 2\pi\cdot\frac{df}{d\beta(f)}|_{f=f_0}. \tag{4}$$

is the group velocity. Meanwhile, the slope of dispersion curve can be calculated by

$$k(f) = \frac{df}{d\beta(f)}|_{f=f_0}. \tag{5}$$

By comparing (4) and (5), one has

$$V_g(f) = 2\pi\cdot k(f). \tag{6}$$

From (3) to (6), it is known that scanning rate is inversely proportional to the slope of dispersion curve, or the group velocity. It can thus be written as: $\nu(f) \propto 1/k(f)$ or $\nu(f) \propto 1/V_g(f)$. This clearly indicates that a high scanning rate requires a very dispersive guiding structure. Therefore, for

enhancing angle scanning rate, certain features should be added to a guiding structure, which may lead to a large dispersion.

However, a slow-wave structure does not radiate under its fundamental mode. In order to convert a slow wave mode to a leaky wave mode, periodic perturbations are introduced into the structure. It leads to an infinite number of space harmonics [1], whose propagation constants $\beta_n(f)$ are given by

$$\beta_n(f) = \beta(f) + \frac{2\pi n}{p}, \quad n = 0, \pm 1, \pm 2, \cdots \tag{7}$$

where p is the period of modulation. One usually employs $n = -1$ space harmonic for radiation. In this case, the propagation constant is

$$\beta_{-1}(f) = \beta(f) - \frac{2\pi}{p}. \tag{8}$$

For this space harmonic to radiate, $\beta_{-1}(f) < k_0$ condition should be fulfilled.

Although the energy is radiated by the first space harmonic β_{-1}, scanning rate of antenna is still same as the fundamental mode,

$$v_{-1}(f) = v(f). \tag{9}$$

Periodic modulation only shifts the dispersion curve without changing a large dispersion characteristic. Therefore, slowing down the group velocity of a slow-wave feeding line is a way to enhance the scanning rate of its leaky-wave radiation.

B. BROADSIDE OPEN STOPBAND SUPPRESSION

Periodically modulated leaky wave antennas usually have a low radiation efficiency at the broadside frequency. This phenomenon is known as *open stopband*, since most of the incident power is constructively reflected back to the source. It can be explained through an even-odd mode based illustration given in Fig.1.

Let us consider an antenna that is able to continuously scan through the broadside with high efficiency. In this case, the antenna must maintain a traveling wave along the structure at the broadside frequency. Since a traveling-wave field changes its profile with time, one may decompose it into even mode and odd mode, which corresponds to the voltage distribution in Fig.1(a). To avoid radiation efficiency drop at the broadside, both even and odd modes should radiate efficiently so that the radiation maintains all the time. In summary, for a high radiation efficiency at the broadside frequency, a leaky wave antenna should have efficient radiation under both even and odd field excitations.

For a symmetric structure in Fig.1(b), the field distributions of unit cell under even and odd excitations are illustrated. It is clearly seen that there exists residual polarization in the longitudinal direction under an odd mode excitation. However, on the other hand, a perfect cancellation in the longitudinal direction can be noted for an even mode. This explains why the symmetric leaky-wave antenna inevitably suffers from a radiation drop at the broadside.

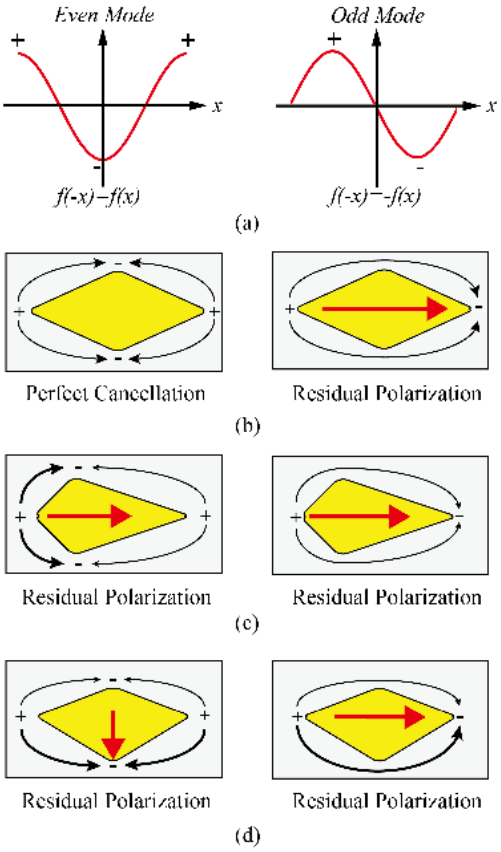

FIGURE 1. Unit-cell electric field distribution at broadside under even and odd mode excitations: (a) voltage distribution, (b) symmetric geometry, (c) transversally asymmetric shape, (d) longitudinally asymmetric shape.

The above insight leads to a straightforward design guideline to avoid the radiation efficiency drop at the broadside. If the symmetry of structure is broken, it is possible to produce a residual polarization for even mode, and hence improve its radiation efficiency. Fig.1(c) and (d) show two approaches to break the symmetry, where the former breaks the transversal symmetry and the latter breaks the longitudinal symmetry. By carefully tuning the asymmetries, one is able to equalize the radiation efficiencies of even and odd modes, so as to completely suppress the open stopband at the broadside radiation.

III. PROPOSED CONFIGURATION

The proposed dispersive slow-wave structure for a high scanning rate is shown in Fig.2. Basically, it consists of an SIW with 45° inclined slots on both top and bottom layers. High-density slots slow down both phase and group velocities of the guided wave, and 45° incline enforces the fields to be polarized in 45° direction. As illustrated in Sec. II-A, such a slow-group-velocity feeding line is the key to realize high scanning rate leaky-wave radiation.

The substrate is Rogers RT 5880 printed circuit broad, which has thickness $h = 0.508$ mm, relative dielectric constant $\varepsilon_r = 2.2$, and loss tangent $\tan\delta = 0.0009$.

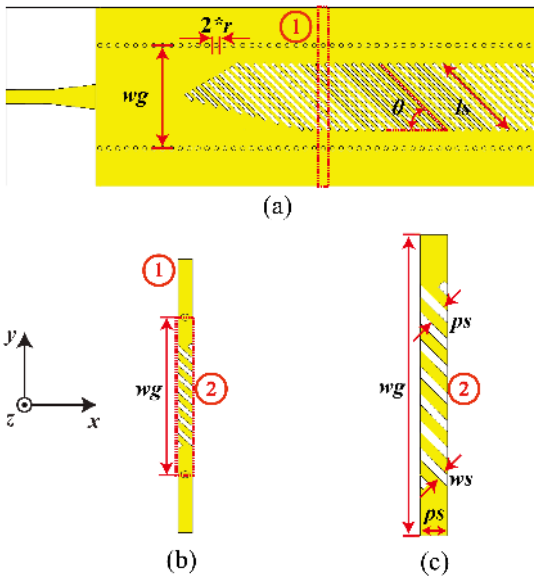

FIGURE 2. The proposed SIW slow-wave transmission structure: (a) overall feeding line, (b) unit cell with two SIW via holes, (c) unit cell model used for simulation (where via holes have been replaced with perfect electric walls).

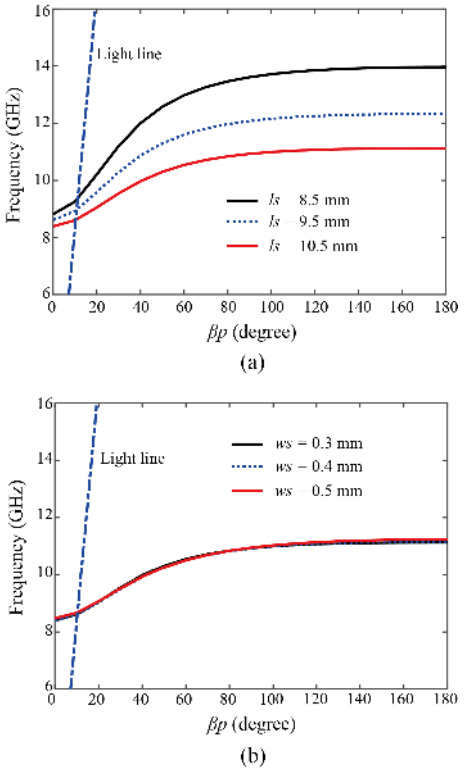

FIGURE 3. Effect of geometrical parameters on dispersion diagram of proposed structure: (a) slot length *ls*, (b) slot width *ws*.

The radius of metallic vias is $r = 0.25$ mm, the width of waveguide is $wg = 11.5$ mm, and the period of vias is $ps = 1$ mm. The length, width, period and rotating angle of slots are $ls = 10.5$ mm, $ws = 0.3$ mm, $ps = 1$ mm, and $\theta = 45°$, respectively. Dispersion diagram of a unit cell has been calculated through the Eigenmode Mode Solver of CST Microwave Studio (MWS). Boundary conditions of unit cell with and without modulation are set as periodic, perfect electric conductor (PEC), and PEC, along x-, y-, and z-axes, respectively. Sweeping parameter is set as the propagation phase of travelling wave. To reduce analysis complexity and calculation time, in the simulation model, unit cell of the slotted slow wave SIW showing in Fig.2(b) is replaced with the one shown in Fig.2(c).

The dispersion curves of simplified unit cell are given in Fig.3. The length of slots ls determines the upper cut-off frequency of slotted SIW. As the length increases, the upper cut-off frequency reduces. However, the lower cut-off frequency undergoes a small shift only. Fig.3(b) presents the influence of slot width on propagation constant. When the width increases, the dispersion curves are almost the same without any change. Based on our parametric study, we select length $ls = 10.5$ mm and the width $ws = 0.3$ mm for designing high scanning rate antennas. The slope of the corresponding dispersion curve is small enough to slow down the group velocity and hence to achieve a high scanning rate.

Since the small-slope part of the dispersion curve in Fig.3 lies in the slow-wave region, it does not radiate. Therefore, to excite leaky-wave radiation, a periodic modulation needs to be applied to the slow-wave slotted SIW. Since the period of this modulation p is related with the broadside frequency f_b, we first need to select a proper broadside frequency. f_b should be chosen as less than the upper cut-off frequency, which from Fig.3(b), is noted as $f_{up} = 11.1$ GHz (when $ls = 10.5$ mm). Based on that, we let $f_b = 10.5$ GHz. The period of modulation turns out to be $p = 18$ mm. Our modulation scheme is explained as follows.

There are 18 sub unit-cells in the unit-cell, since the period of single slot and unit cell are $ps = 1$ mm and $p = 18$ mm, respectively. The unit cell exhibits an anti-symmetric shape, which is divided into two groups of slots above and below the longitudinal center axis, as shown in Fig.4(a). The lengths of slots are denoted as h_1 to h_{18} in a left to right sequence, in the upper group. In the lower group, their sequence is reversed as h_{18} to h_1. The slot length gradually increases from h_1 to h_{13}, where $h_{13} = ls/2$, and then decreases till $h_{18} = ls/12$. After fixing these lengths, all the slots of a unit-cell, are rotated by an angle $\theta = 45°$. It thus transforms the unit-cell shape of Fig.4(a) to that in Fig.4(b), which basically forms a symmetric rhombus structure.

In a periodically modulated symmetric structure, there still exhibits an open stopband, which can be closed by introducing asymmetry into the structure, as explained above in Sec. II. Our asymmetric unit-cell shapes are shown in Fig.4(c) and Fig.4(d). They have been designed through the same procedure of setting lengths and rotating slots, as explained above for the case of symmetric unit-cell. Only the sequence of length has been altered by a distance d, which refers to the separation between the tallest slot and the line passing

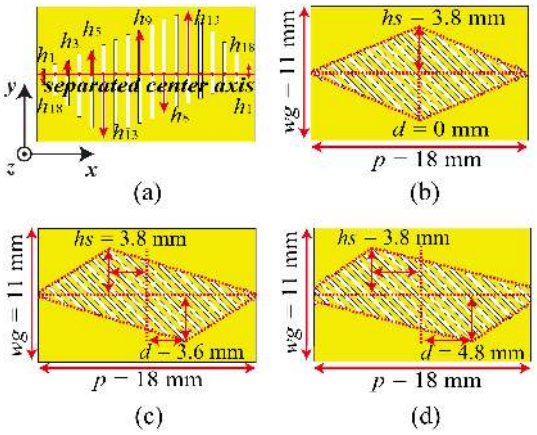

FIGURE 4. Evolution of an asymmetric shape: (a) original symmetrical unit-cell with vertical slots, $d = 0$ mm, $hs = 3.8$ mm; (b) symmetric unit-cell after slots are rotated by 45°, $d = 0$ mm, $hs = 3.8$ mm; (c) asymmetric unit-cell with rotated slots, $d = 3.6$ mm, $hs = 3.8$ mm; (d) asymmetrical unit-cell with rotated slots, $d = 4.8$ mm, $hs = 3.8$ mm.

TABLE 1. Lengths of symmetric and asymmetric unit cell slots in Fig.4.

Symbol	Fig.4(a), (b)	Fig.4(c)	Fig.4(d)
h_1	$e \cdot 1/13$	$e \cdot 1/10$	$e \cdot 2/10$
h_2	$e \cdot 2/13$	$e \cdot 2/10$	$e \cdot 3/10$
h_3	$e \cdot 3/13$	$e \cdot 3/10$	$e \cdot 4/10$
h_4	$e \cdot 4/13$	$e \cdot 4/10$	$e \cdot 5/10$
h_5	$e \cdot 5/13$	$e \cdot 5/10$	$e \cdot 6/10$
h_6	$e \cdot 6/13$	$e \cdot 6/10$	$e \cdot 7/10$
h_7	$e \cdot 7/13$	$e \cdot 7/10$	$e \cdot 8/10$
h_8	$e \cdot 8/13$	$e \cdot 8/10$	$e \cdot 9/10$
h_9	$e \cdot 9/13$	$e \cdot 9/10$	$e \cdot 10/10$
h_{10}	$e \cdot 10/13$	$e \cdot 10/10$	$e \cdot 10/10$
h_{11}	$e \cdot 11/13$	$e \cdot 8/9$	$e \cdot 9/10$
h_{12}	$e \cdot 12/13$	$e \cdot 7/9$	$e \cdot 8/10$
h_{13}	$e \cdot 13/13$	$e \cdot 6/9$	$e \cdot 7/10$
h_{14}	$e \cdot 5/6$	$e \cdot 5/9$	$e \cdot 6/10$
h_{15}	$e \cdot 4/6$	$e \cdot 4/9$	$e \cdot 5/10$
h_{16}	$e \cdot 3/6$	$e \cdot 3/9$	$e \cdot 4/10$
h_{17}	$e \cdot 2/6$	$e \cdot 2/9$	$e \cdot 3/10$
h_{18}	$e \cdot 1/6$	$e \cdot 1/9$	$e \cdot 2/10$
$e = ls/2$	5.25 mm		

through the center of unit-cell. An increased d refers to an increased asymmetry, whereas $d = 0$ mm refers to a symmetric unit-cell. Detailed parameters of the unit-cell shapes of Fig.4 are listed in Table 1.

To find the best asymmetry or an optimum d (for closing the stopband), we carry out a dispersion analysis of our unit-cells, for different values of d. These results are presents in Fig.5. It can be clearly seen that there exists an open stopband for a symmetric unit-cell ($d = 0$ mm), which can be closed as the unit-cell shape is made asymmetric by increasing $d = 4.8$ mm. This is inline with the concepts presented in Sec. II.

Suppressing of band gap can also be understood and verified through a electric field analysis of the structure, as given in Fig.6. These field distributions under even and odd mode excitations, have been obtained from CST MWS. Electric field patterns have been examined for three frequency points,

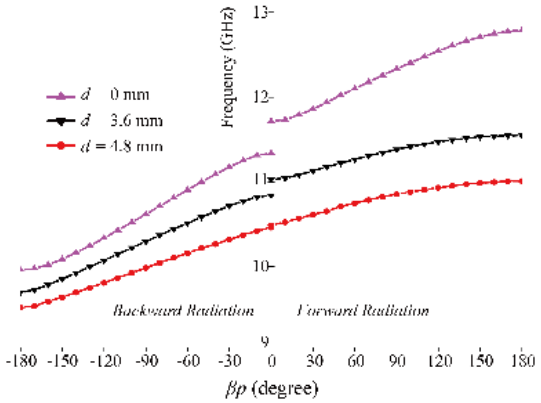

FIGURE 5. Comparison of dispersion diagrams for symmetric and asymmetric unit-cells.

11.5 GHz, 10.9 GHz, and 10.5 GHz. They refer to the broadside radiation points of the three cases compared in Fig. 5. Figs. 6(a) and (b), show that field distributions of the unit cell in Fig.4(b) under odd and even mode excitations, respectively. It can be noted that the field distribution has a residual radiation, whose polarization is vertical to the slots under odd mode. On the other hand, they are almost cancelled at center of the unit-cell, under an even mode excitation. This can be seen through two opposite trapezoidal circling regions in Fig.6(b). Cancellation of fields results in a lower efficiency of the antenna structure, as explained above in Sect. II. A similar situation is noted for the case of Fig.4(c) at 10.9 GHz. Although, the unit-cell shape is asymmetric, it is still not able to avoid a cancellation of fields, when $d = 3.6$ mm. It is only when the asymmetry is sufficiently increased at $d = 4.8$, the band gap of two modes is closed at 10.5 GHz. There has a residual radiation for both field distributions in Figs. 6(e) and (f). The residual radiation under the odd mode excitation has the same polarization as that of Fig. 6(a) and (c), which is perpendicular to the slots. For even mode excitation, Fig. 6(f) shows two triangle circling areas with the same direction and different magnitude of field distribution. Existence of more residual fields leads to an enhanced efficiency, and hence a closed stop band for broadside radiation.

IV. DESIGN EXAMPLES

A. 45° LINEARLY POLARIZED LWA

Using the unit-cell shape evolved above in Fig.4(d), we have designed a 45° LP LWA. It is shown in Fig.7. Its length and width are $Lr = 240$ mm, $w = 20$ mm. It consists of 11 unit-cells, and two microstrip lines which provide its interface with coaxial connectors. For an improved matching, part of the microstrip line is also tapered before joining it with the top surface of SIW.

The simulated S-parameters and total efficiency of 45° LP LWA is presented in Fig.8(a). Here, the S_{11} is below -10 dB from 9.9 GHz to 11.1 GHz, which implies that the stopband has been completely closed. This frequency range (9.9 - 11.1 GHz) corresponds to both forward and

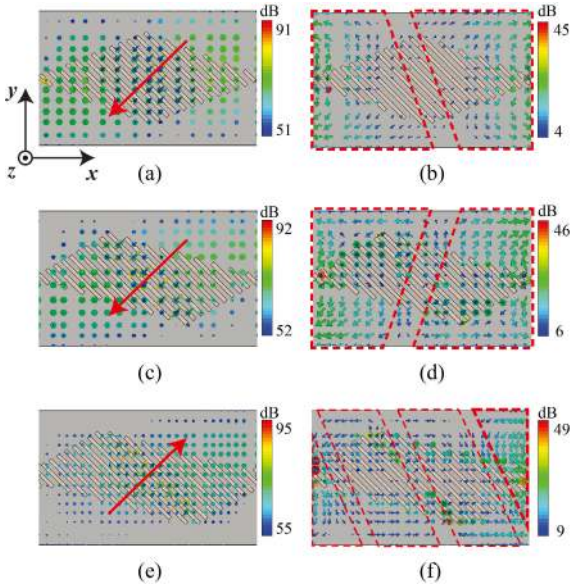

FIGURE 6. Field distributions of symmetric and asymmetric unit-cells under odd and even mode excitations: (a) odd mode (d = 0 mm, f = 11.5 GHz); (b) even mode (d = 0 mm, f = 11.5 GHz); (c) odd-mode (d = 3.6 mm, f = 10.9 GHz); (d) even mode (d = 3.6 mm, f = 10.9 GHz); (e) odd mode (d = 4.8 mm, f = 10.5 GHz); (f) even mode (d = 4.8 mm, f = 10.5 GHz).

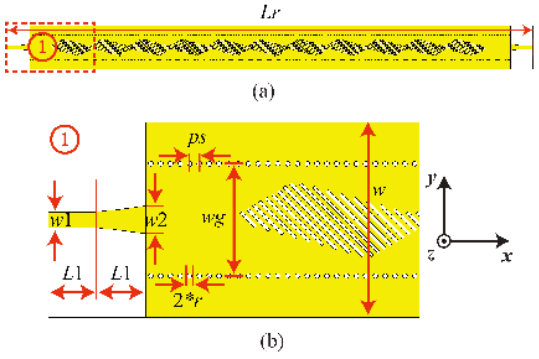

FIGURE 7. Our designed 45° LP LWA, (a) Top view, (b) Closer view of the input port, ($w1$ = 1.6 mm, $L1$ = 5 mm, $w2$ = 2.8 mm, wg = 11.5 mm, r = 0.25 mm, ps = 1 mm).

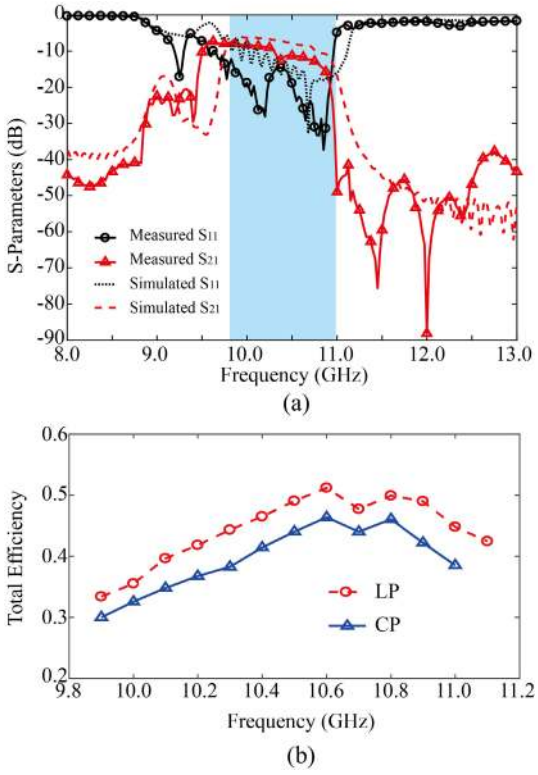

FIGURE 8. (a)Measured and simulated S-parameters of 45° LP LWA. (b) The efficiency of LP and CP LWAs.

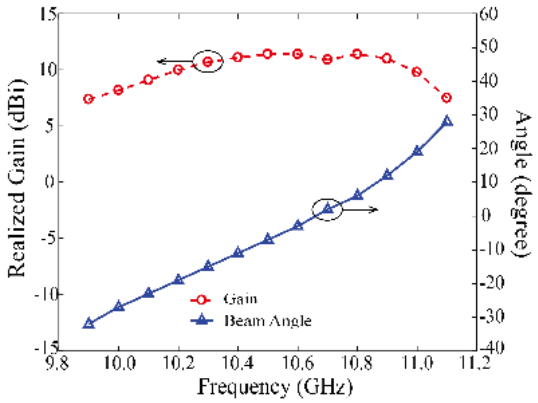

FIGURE 9. Simulated peak gain, and scanning direction of 45° LP LWA.

backward radiation. The span cover the broadside at around 10.7 GHz, which well agrees with the predicted broadside point at 10.5 GHz seen for d = 4.8 mm in Fig.5. The small deviation may be attributed to a finite size of leaky-wave antennas. A periodical unit cell assumes an infinite periodic structure, which is not possible to realize practically. A finite periodic structure has edge effects, and its results are expected to deviate a little from those obtained from a unit-cell dispersion curve. The efficiency of two proposed LWAs is shown in Fig.8(b).

The main beam direction and gain of this LWA, are displayed in Fig.9. The beam scanning range of this LWA is from −32° at 9.9 GHz to 28° at 11.1 GHz, and the angle scanning rate is about 50°/GHz. It exhibits a maximum gain 11.43 dBi at 10.5 GHz, and a nearly flat gain from 10.2 GHz to 11.0 GHz.

Fig.10 presents the normalized radiation patterns in x-o-z plane at three different frequency points. It is seen that the beam scans continuously from backward to forward across the broadside, which is consistent with the results of Fig.9.

B. CIRCULARLY POLARIZED LWA

Our scheme for realizing a circularly polarized (CP) antenna is shown in Fig.11(c). We have combined two linearly polarized antennas through a 3-dB coupler, which also provides a 90° phase shift required for CP operation. The two 45° LP

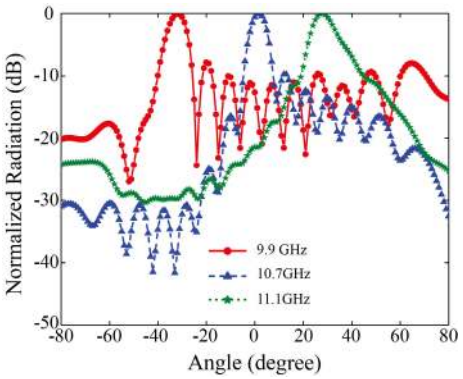

FIGURE 10. Simulated radiation patterns of the 45° LP LWA.

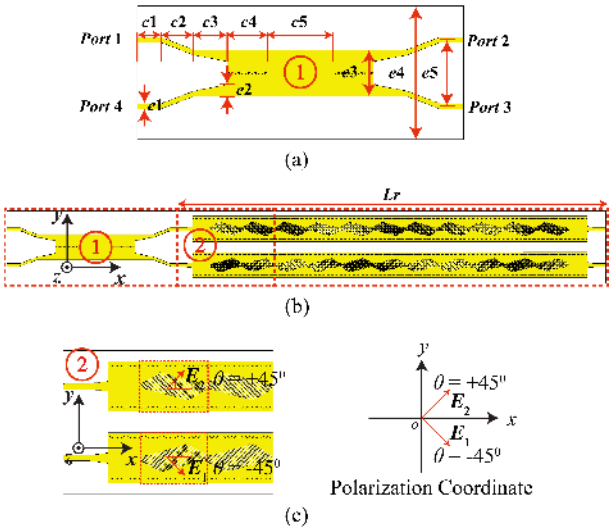

FIGURE 11. The designed CP LWA: (a) top view of the feeding coupler ($c1 = 7$ mm, $c2 = c3 = 10$ mm, $c4 = 12$ mm, $c5 = 20$ mm, $e1 = 1.6$ mm, $e2 = 3.5$ mm, $e3 = 14$ mm, $e4 = 40$ mm, $e5 = 20$ mm, $r = 0.25$ mm); (b) top view of the combined structure; (c) a closer view highlighting the polarization vectors of the two LP LWAs.

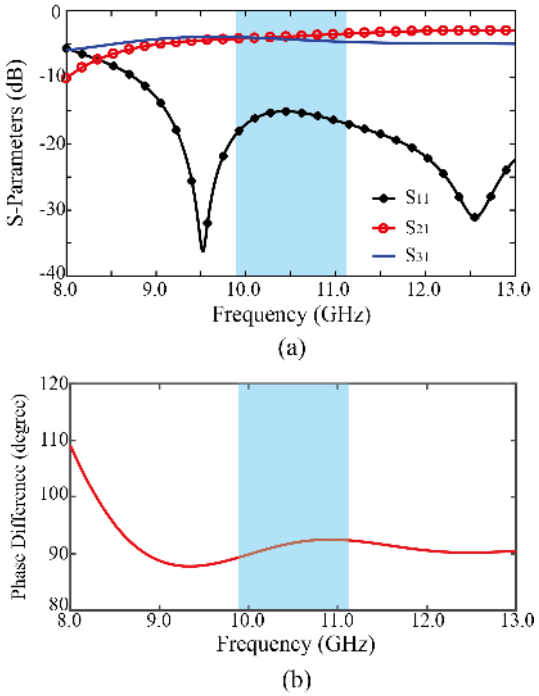

FIGURE 12. Simulation results of the coupler used in our CP LWA, (a) S-parameters, (b) Phase difference between ports 2 and 3.

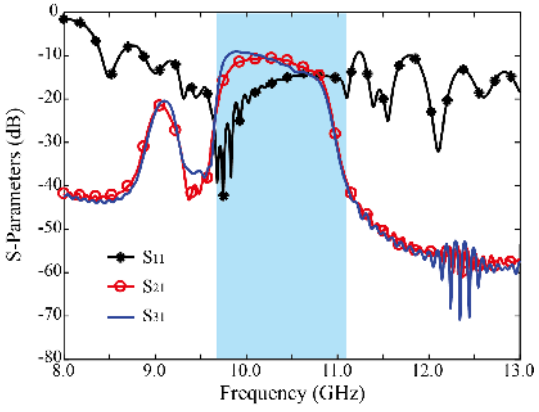

FIGURE 13. Simulated S-parameters of our CP LWA.

LWAs, similar to that of Sect. III-A, are placed in a parallel orientation. They radiate $\theta = +45°$ and $\theta = -45°$ polarized beams. When they are fed in equal amplitude and a 90° phase shift, it results in CP radiation. The coupler for equal power division and 90° phase shift is shown in Fig.11(a). Fig.12 shows the simulated S-parameters and phase differences of this coupler. It clearly exhibits a good reflection (below −15 dB), equal power division, and an about 90° phase difference in the frequency range 9.0-13.0 GHz.

For the designed CP LWA, the simulated S-parameters are displayed in Fig.13. It is seen that the reflection coefficient is below −16 dB from 9.5 to 11.1 GHz. Transmission coefficients of port 2 and 3 (S_{21}, S_{31}) are both below −10 dB within 9.7-11.1 GHz, which implies that most of the energy has leaked out of the structure, and only a very small part of it reached the two end ports.

Simulated beam gain, axial ratio (AR), and beam directions of the CP LWA are presented in Fig.14 and Fig.20. In Fig.20, it is seen that the CP LWA has an AR below 3 dB, in a wide frequency band from 10.1 GHz to 11.0 GHz. From Fig.14, the CP LWA scans from −31° at 9.9 GHz to 21° at 11.0 GHz. The gain of CP LWA is almost flat from 9.9 GHz to 11 GHz.

Fig.15 shows the normalized radiation patterns in x-o-z plane at three different frequency points. It is seen that the beam scans continuously from backward to forward across the broadside, which is consistent with the results in Fig.14. Similar to the LP antenna, the broadside radiation frequency is around 10.7 GHz. Around the main beam, side-lobe levels are different on the right and left sides. This asymmetry of radiation pattern is actually expected from the asymmetric field distribution of guided waves (or equivalently surface currents), along the radiating aperture of

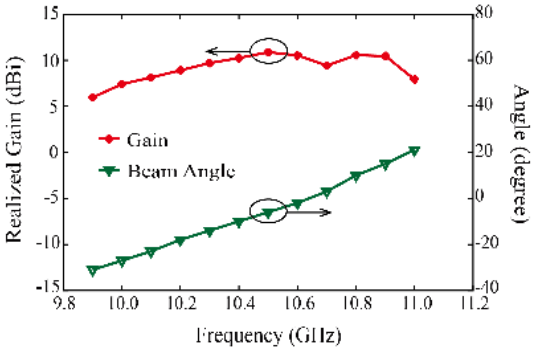

FIGURE 14. Simulation results of our CP LWA realized gain,and scanning angle.

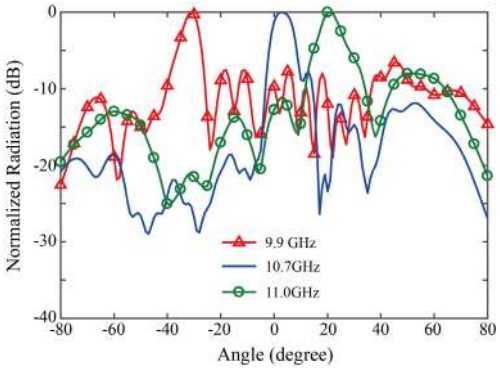

FIGURE 15. Simulated radiation patterns of our CP LWA.

a leaky-wave antenna. It is known that energy leaks out gradually as the incident signal propagates along the structure. Based on that, strong fields (and hence surface currents) exist near the port of excitation. Their amplitudes are much reduced towards the opposite port, where residual energy is absorbed in a matched load.

V. EXPERIMENTAL VALIDATION

The two designed LWAs were fabricated and tested. The fabricated prototypes are shown in Fig.16. During measurements, an antenna was fed at its input port through an SMA connector, while other ports were terminated in a 50Ω load. Performance of these prototype antennas is discussed as follows.

A. 45° LP LWA

Measured S-parameters of 45° LP LWA have already been presented in Fig.8. A good match with simulation results is seen there. A small frequency shift is observed between the two results. It may be attributed to the tolerance of dielectric permittivity. Measured reflection coefficients presents a crest around broadside, however, it still remains lower than −10 dB, in the scanning band of 9.6-10.8 GHz.

Measured gain and the main beam directions are given in Fig.17. It shows a beam scanning range of −33° at 9.6 GHz to 28° at 10.8 GHz, which is consistent with simulation

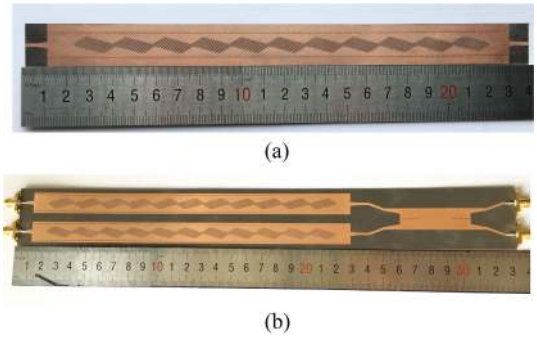

FIGURE 16. Photograph of two fabricated prototypes, (a) LP LWA, (b) CP LWA.

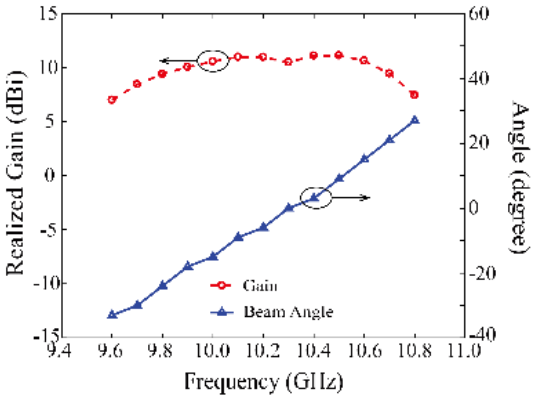

FIGURE 17. Measured gain and scanning direction of our LP LWA.

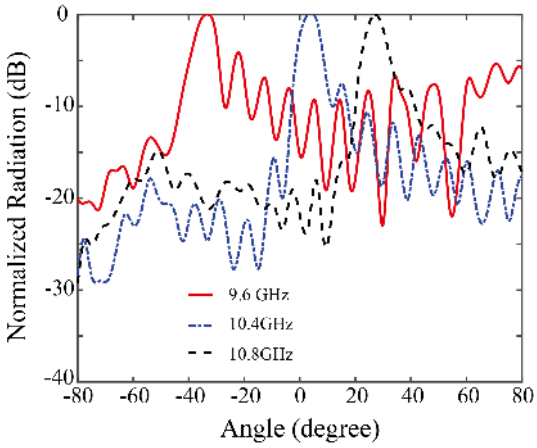

FIGURE 18. Measured radiation patterns of our LP LWA.

results. A small frequency shift is observed, which may be attributed to the tolerance of dielectric permittivity or to a fabrication error. A maximum gain of 11.12 dBi is noted at 10.5 GHz. The gain changes within the frequency range of 9.7 GHz and 10.7 GHz. Afterwards, it sharply drops to 7.01 dBi and 7.45 dBi, beyond the extreme scanning angles of backward and forward directions, respectively.

Fig.18 gives normalized radiation patterns of this LP LWA in the x-o-z plane at three different frequency points. As seen

TABLE 2. Comparsion of scanning rates for reported works, exhibiting closed stopband situation.

Reported Works	Range and Efficiency (degree)	Bandwidth and Frequency (GHz)	Rate (degree/GHz)	Polarization LP or CP	Implementation Technique and One or Two Face	Closed Broadside Stopband Yes or No
[19]	$72-NA$	$28.6\%\ (7.5-10.0)$	28.8	CP	SIW by One Face	Yes
[22]	$124.5-40\%$	$24.1\%\ (12.25-15.6)$	37.2	LP	SIW by One Face	Yes
[23]	$119-90\%$	$37.8\%\ (7.7-11.0)$	35	LP	SIW by Two Face	Yes
[25]	$32-92\%$	$36.4\%\ (9-13)$	8	LP	Microstrip by One Face	Yes
[27]	$36-NA$	$8.3\%\ (23-25)$	18	CP	Microstrip by Two Face	Yes
[28]	$27-85\%$	$8\%\ (2.4-2.6)$	135	LP	Microstrip by Two Face	No (Only forward)
[30]	$35-NA$	$2.9\%\ (13.5-13.9)$	87.5	LP	SIW by One Face	No (Only forward)
[31]	$123-NA$	$4.5\%\ (10.6-11.6)$	123	LP	SIW by Two Face	Yes
This work	$61-50\%$	$11.7\%\ (9.6-10.8)$	50.8	45^0 LP	SIW by One Face	Yes
This work	$52-45\%$	$9.7\%\ (9.8-10.8)$	52	CP	SIW by One Face	Yes

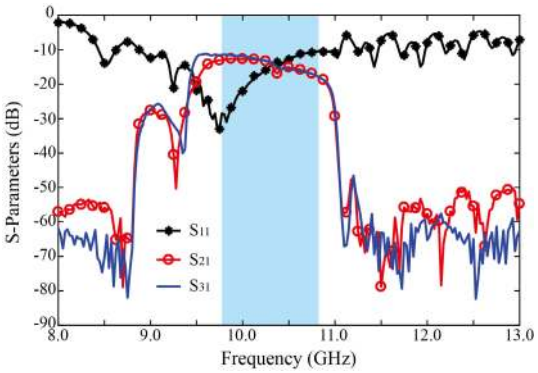

FIGURE 19. Measured S-parameters of our CP LWA.

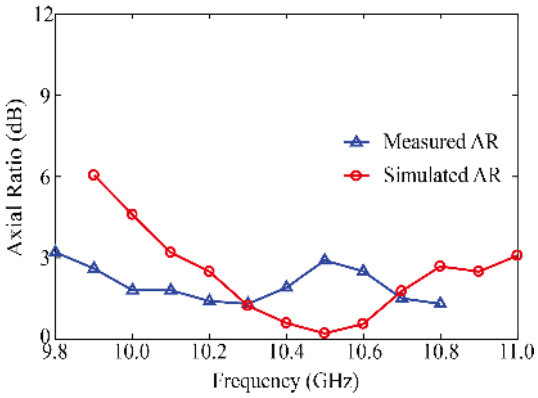

FIGURE 20. Simulated and measured axial ratios of our CP LWA.

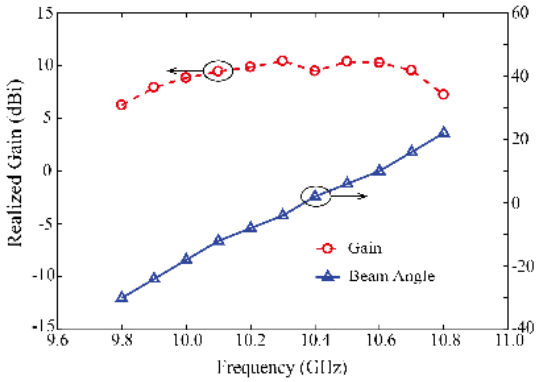

FIGURE 21. Measured gain, and scanning angles of our CP LWA.

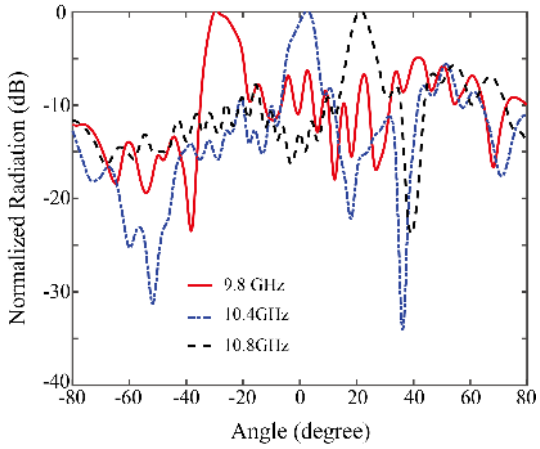

FIGURE 22. Measured radiation patterns of our CP LWA.

here, the main beam scans continuously from backward to forward across the broadside. These results are consistent with those in Fig.17.

B. CP LWA

Fig.19 presents measured S-parameters of our CP LWA. They match well with those obtained through simulation. As desired, all the measured parameters are below -10 dB from 9.5 GHz to 11.0 GHz. It indicates that the open stopband has been closed.

Measured AR of the CP LWA is shown in Fig.20. It is seen that AR stays below -3.1 dB from 9.8 GHz to 10.8 GHz, which basically confirms an existence of circular polarization in this band. As shown in Fig.21, the LWA scans from $-30°$ at 9.8 GHz to 22° at 10.8 GHz. The measured gain of CP LWA maintains a flat value from 9.9 GHz to 10.7 GHz. Afterwards, it drops to 6.03 dBi beyond the extreme angle of backward direction.

Fig.22 presents normalized radiation patterns in x-o-z plane at three frequencies. As seen here, the main beam scans continuously from backward to forward across the broadside. These results are consistent with those in Fig.21.

To demonstrate the superiority of our antennas, we compare them with other previous works, as listed in Table 2.

It is seen from this comparison that our LWAs have a higher scanning rate among 45° linearly polarized and circular polarized candidates. Our antennas have a continuous scanning range from backward to forward directions, without an open stopband at broadside. However, it should be pointed out that the scanning range of our LWAs is relatively small, and slightly larger than 60° only. Based on that, these antennas are suitable for those imaging applications where a very broad view or a large angular span is not required.

VI. CONCLUSION

In this paper, a new class of 45° LP and CP LWAs has been explored, to obtain a very high scanning rate, and a closed stopband simultaneously. These two features are known to be attractive for imaging applications. The proposed structure was derived from an SIW, by making closely spaced inclined slots on its top wall. This led to a highly dispersive characteristic, which is desired for a high scanning rate of a resulting LWA. Further, carefully designed asymmetric periodic modulation was applied on this slotted structure. It was shown that the proposed modulation effectively solves the well-known open stopband problem, which otherwise results in a low efficiency at broadside. To demonstrate the principles and proposed techniques, two design examples were fabricated. Measured results confirm the high scanning rate, and closed stopband, features of our antennas. Based on that, the proposed LWAs with different polarization appear potential candidates for high-performance imaging applications. A single antenna is suitable for one-dimensional scanning. Combining two of them can also lead to a two-dimensional imaging system. The scan range of LP LWA is from $-33°$ to $28°$ in at 9.6 - 10.8 GHz band. For CP LWA, it is $-30°$ to $22°$, for a frequency span of 9.8 - 10.8 GHz. This may limit its applications in some imaging scenarios, where a larger view, or a full half-space scanning is required.

REFERENCES

[1] D. R. Jackson, C. Caloz, and T. Itoh, "Leaky-wave antennas," *Proc. IEEE*, vol. 100, no. 7, pp. 2194–2206, Mar. 2012.

[2] A. A. Oliner, D. R. Jackson, and J. L. Volakis, *Antenna Engineering Handbook*. New York, NY, USA: McGraw-Hill, 2007.

[3] J. Esch, "Leaky-wave theory, techniques, and applications: From microwaves to visible frequencies," *Proc. IEEE*, vol. 103, no. 5, pp. 789–792, May 2015.

[4] P. Antonik, M. C. Wicks, H. D. Griffiths, and C. J. Baker, "Frequency diverse array radars," in *Proc. IEEE Conf. Radar*, Apr. 2006, p. 3.

[5] S. Gupta, S. Abielmona, and C. Caloz, "Microwave analog real-time spectrum analyzer (RTSA) based on the spectral–spatial decomposition property of leaky-wave structures," *IEEE Trans. Microw. Theory Techn.*, vol. 57, no. 12, pp. 2989–2999, Dec. 2009.

[6] B. Husain, M. Steeg, and A. Stohr, "Estimating direction-of-arrival in a 5G hot-spot scenario using a 60 GHz leaky-wave antenna," in *Proc. IEEE Int. Conf. Microw., Antennas, Commun. Electron. Syst. (COMCAS)*, Nov. 2017, pp. 1–4.

[7] K. M. Morshed, D. K. Karmokar, and K. P. Esselle, "Highly efficient leaky-wave antenna array for 28-GHz millimeter-wave terminals," in *Proc. IEEE 85th Veh. Technol. Conf. (VTC Spring)*, Jun. 2017, pp. 1–4.

[8] F. M. Monavar, S. Shamsinejad, R. Mirzavand, J. Melzer, and P. Mousavi, "Beam-steering SIW leaky-wave subarray with flat-topped footprint for 5G applications," *IEEE Trans. Antennas Propag.*, vol. 65, no. 3, pp. 1108–1120, Mar. 2017.

[9] J. Hunt, T. Driscoll, A. Mrozack, G. Lipworth, M. Reynolds, D. Brady, and D. R. Smith, "Metamaterial apertures for computational imaging," *Science*, vol. 339, no. 6117, pp. 310–313, Jan. 2013. [Online]. Available: http://science.sciencemag.org/content/339/6117/310.abstract

[10] T. Sleasman, M. Boyarsky, L. Pulido-Mancera, T. Fromenteze, M. F. Imani, M. S. Reynolds, and D. R. Smith, "Experimental synthetic aperture radar with dynamic metasurfaces," *IEEE Trans. Antennas Propag.*, vol. 65, no. 12, pp. 6864–6877, Dec. 2017.

[11] O. Yurduseven, D. L. Marks, T. Fromenteze, and D. R. Smith, "Dynamically reconfigurable holographic metasurface aperture for a mills-cross monochromatic microwave camera," *Opt. Express*, vol. 26, no. 5, pp. 5281–5291, Mar. 2018.

[12] A. V. Diebold, M. F. Imani, T. Sleasman, and D. R. Smith, "Phaseless computational ghost imaging at microwave frequencies using a dynamic metasurface aperture," *Appl. Opt.*, vol. 57, no. 9, pp. 2142–2149, Mar. 2018.

[13] J. Liu, D. R. Jackson, and Y. Long, "Substrate integrated waveguide (SIW) leaky-wave antenna with transverse slots," *IEEE Trans. Antennas Propag.*, vol. 60, no. 1, pp. 20–29, Jan. 2012.

[14] J. Liu, X. Tang, Y. Li, and Y. Long, "Substrate integrated waveguide leaky-wave antenna with H-Shaped slots," *IEEE Trans. Antennas Propag.*, vol. 60, no. 8, pp. 3962–3967, Aug. 2012.

[15] J. Liu, D. R. Jackson, Y. Li, C. Zhang, and Y. Long, "Investigations of SIW leaky-wave antenna for endfire-radiation with narrow beam and sidelobe suppression," *IEEE Trans. Antennas Propag.*, vol. 62, no. 9, pp. 4489–4497, Sep. 2014.

[16] C. Caloz and T. Itoh, *Electromagnetic Metamaterials: Transmission Line Theory and Microwave Applications*. Hoboken, NJ, USA: Wiley, 2005.

[17] Y. Dong and T. Itoh, "Composite Right/Left-handed substrate integrated waveguide and half mode substrate integrated waveguide leaky-wave structures," *IEEE Trans. Antennas Propag.*, vol. 59, no. 3, pp. 767–775, Mar. 2011.

[18] N. Nasimuddin, Z. N. Chen, and X. Qing, "Substrate integrated metamaterial-based leaky-wave antenna with improved boresight radiation bandwidth," *IEEE Trans. Antennas Propag.*, vol. 61, no. 7, pp. 3451–3457, Jul. 2013.

[19] Y. Dong and T. Itoh, "Substrate integrated composite right-/left-handed leaky-wave structure for polarization-flexible antenna application," *IEEE Trans. Antennas Propag.*, vol. 60, no. 2, pp. 760–771, Feb. 2012.

[20] J. T. Williams, P. Baccarelli, S. Paulotto, and D. R. Jackson, "1-D combline leaky-wave antenna with the open-stopband suppressed: Design considerations and comparisons with measurements," *IEEE Trans. Antennas Propag.*, vol. 61, no. 9, pp. 4484–4492, Sep. 2013.

[21] Y.-L. Lyu, X.-X. Liu, P.-Y. Wang, D. Erni, Q. Wu, C. Wang, N.-Y. Kim, and F.-Y. Meng, "Leaky-wave antennas based on noncutoff substrate integrated waveguide supporting beam scanning from backward to forward," *IEEE Trans. Antennas Propag.*, vol. 64, no. 6, pp. 2155–2164, Jun. 2016.

[22] J. Liu, W. Zhou, and Y. Long, "A simple technique for open-stopband suppression in periodic leaky-wave antennas using two nonidentical elements per unit cell," *IEEE Trans. Antennas Propag.*, vol. 66, no. 6, pp. 2741–2751, Jun. 2018.

[23] D. K. Karmokar, Y. J. Guo, P.-Y. Qin, S.-L. Chen, and T. S. Bird, "Substrate integrated waveguide-based periodic Backward-to-Forward scanning leaky-wave antenna with low cross-polarization," *IEEE Trans. Antennas Propag.*, vol. 66, no. 8, pp. 3846–3856, Aug. 2018.

[24] S.-L. Chen, D. K. Karmokar, P.-Y. Qin, R. W. Ziolkowski, and Y. J. Guo, "Polarization-reconfigurable leaky-wave antenna with continuous beam scanning through broadside," *IEEE Trans. Antennas Propag.*, vol. 68, no. 1, pp. 121–133, Jan. 2020.

[25] X.-L. Tang, Q. Zhang, S. Hu, Y. Zhuang, A. Kandwal, G. Zhang, and Y. Chen, "Continuous beam steering through broadside using asymmetrically modulated goubau line leaky-wave antennas," *Sci. Rep.*, vol. 7, no. 1, p. 11685, Dec. 2017.

[26] S. Otto, A. Al-Bassam, A. Rennings, K. Solbach, and C. Caloz, "Transversal asymmetry in periodic leaky-wave antennas for bloch impedance and radiation efficiency equalization through broadside," *IEEE Trans. Antennas Propag.*, vol. 62, no. 10, pp. 5037–5054, Oct. 2014.

[27] S. Otto, Z. Chen, A. Al-Bassam, A. Rennings, K. Solbach, and C. Caloz, "Circular polarization of periodic leaky-wave antennas with axial asymmetry: Theoretical proof and experimental demonstration," *IEEE Trans. Antennas Propag.*, vol. 62, no. 4, pp. 1817–1829, Apr. 2014.

[28] G. Zhang, Q. Zhang, S. Ge, Y. Chen, and R. D. Murch, "High scanning-rate leaky-wave antenna using complementary microstrip-slot stubs," *IEEE Trans. Antennas Propag.*, vol. 67, no. 5, pp. 2913–2922, May 2019.

[29] D.-F. Guan, P. You, Q. Zhang, K. Xiao, and S.-W. Yong, "Hybrid spoof surface plasmon polariton and substrate integrated waveguide transmission line and its application in filter," *IEEE Trans. Microw. Theory Techn.*, vol. 65, no. 12, pp. 4925–4932, Dec. 2017.
[30] D.-F. Guan, Q. Zhang, P. You, Z.-B. Yang, Y. Zhou, and S.-W. Yong, "Scanning rate enhancement of leaky-wave antennas using slow-wave substrate integrated waveguide structure," *IEEE Trans. Antennas Propag.*, vol. 66, no. 7, pp. 3747–3751, Jul. 2018.
[31] S.-D. Xu, D.-F. Guan, Q. Zhang, P. You, S. Ge, X.-X. Hou, Z.-B. Yang, and S.-W. Yong, "A wide-angle narrowband leaky-wave antenna based on substrate integrated waveguide-spoof surface plasmon polariton structure," *IEEE Antennas Wireless Propag. Lett.*, vol. 18, no. 7, pp. 1386–1389, Jul. 2019.
[32] R. Torrealba-Melendez, J. L. Olvera-Cervantes, and A. Corona-Chavez, "Resolution improvement of an UWB microwave imaging radar system using circular polarization," in *Proc. Int. Conf. Electron., Commun. Comput. (CONIELECOMP)*, Feb. 2014, pp. 189–193.
[33] A. Ahmed, X. Zhao, and A. Bermak, "Polarization imaging for remote sensing," in *Proc. IEEE Microw., Radar Remote Sens. Symp. (MRRS)*, Aug. 2017, pp. 15–18.

JIANWEN ZHONG received the B.S. degree in applied physics and the M.S. degree in material engineering from the Harbin Institute of Technology, Harbin, China, in 2013 and 2016, respectively. He is currently with the Southern University of Science and Technology, China, as a Research Assistant. His current research interests include metamaterials and leaky wave antennas.

AMIR KHURRUM RASHID received the B.S. degree in electronic engineering from the Ghulam Ishaq Khan Institute of Engineering Sciences and Technology, Pakistan, in 2003, and the Ph.D. degree in electrical engineering from Nanyang Technological University, Singapore, in 2011. From 2003 to 2006, he was an Assistant Manager (Technical) with the National Engineering and Scientific Commission, Pakistan. He was with the Institute for Infocomm Research, Singapore, as a Scientist I, from January 2011 to March 2012. He is currently with the Southern University of Science and Technology, China, as a Visiting Professor. His research interests include antennas and periodic structures.

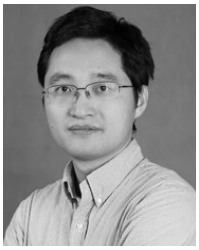

QINGFENG ZHANG (Senior Member, IEEE) received the B.E. degree in electrical engineering from the University of Science and Technology of China (USTC), Hefei, China, in 2007, and the Ph.D. degree in electrical engineering from Nanyang Technological University, Singapore, in 2011. From June 2011 to December 2013, he was with the Poly-Grames Research Center, Ecole Polytechnique de Montreal, Montreal, QC, Canada, as a Postdoctoral Fellow. Since December 2013, he has been with the Southern University of Science and Technology (SUSTech), Shenzhen, China, where he is currently an Associate Professor with tenure. His research interests include largely in emerging novel electromagnetics technologies where he has a special interest in dispersion engineering at microwave and millimeter-wave frequencies. He is a Fellow of IET. He is the Vice Chair of the IEEE Antennas and Propagation Society Shenzhen Chapter. He serves as an Associate Editor for IEEE Access.